Journal of Materials Chemistry B

Solute diffusion and partitioning in multi-arm poly(ethylene glycol) hydrogels

Journal:	*Journal of Materials Chemistry B*
Manuscript ID	TB-ART-09-2022-002004.R1
Article Type:	Paper
Date Submitted by the Author:	24-Nov-2022
Complete List of Authors:	Richbourg, Nathan; The University of Texas at Austin, Biomedical Engineering Peppas, Nicholas; The University of Texas at Austin, Chemical Engineering, Biomedical Engineering

Solute diffusion and partitioning in multi-arm poly(ethylene glycol) hydrogels

Nathan Richbourg[1] & Nicholas A. Peppas[1-4]

[1]Department of Biomedical Engineering, University of Texas, Austin, TX 78712, USA.

[2]McKetta Department of Chemical Engineering, University of Texas, Austin, TX 78712, USA.

[3]Division of Molecular Therapeutics and Drug Delivery, College of Pharmacy, University of Texas, Austin, TX 78712, USA.

[4]Departments of Surgery and Pediatrics, Dell Medical School, University of Texas, Austin, TX 78712, USA.

*Corresponding Author Contact: peppas@che.utexas.edu

Abstract

Controlling solute transport in hydrogels is critical for numerous chemical separation applications, tissue engineering, and drug delivery systems. In previous review work, we have pointed out that proposed theoretical models and associated experiments tend to oversimplify the influence of hydrogel structure on solute transport by addressing only the effects of the polymer volume fraction and mesh size of the networks on solute transport. Here, we reexamine these models by experimenting with a library of multi-arm poly(ethylene glycol) (PEG) hydrogels with simultaneous variations in four independent structural parameters. Standardized, high-throughput fluorescence recovery after photobleaching (FRAP) experiments in hydrogels characterize size-dependent solute diffusion and partitioning in each hydrogel formulation. Solute diffusivity dependence on junction functionality shows an influence from network geometry that is not addressed by mesh size-based models, experimentally validating the use of the geometry-responsive mesh radius in solute diffusivity modeling. Furthermore, the Richbourg-Peppas swollen polymer network (SPN) model accurately predicts how three of the four structural parameters affect solute diffusivity in hydrogels. Comparison with the large pore effective medium (LPEM) model showed that the SPN model better predicts solute size and hydrogel structure effects on diffusivity. This study provides a framework for investigating solute transport in hydrogels that will continue to improve hydrogel design for tissue engineering and drug delivery.

Keywords:

Solute transport; hydrogel; mesh size; mesh radius; swollen polymer network model

Introduction

Understanding solute transport in hydrogels is important for molecular separation processes using hydrogel membranes,[1] for controlling drug delivery from hydrogel reservoirs,[2] and for managing cellular communication in hydrogel-based tissue engineering scaffolds.[3] Fluorescence recovery after photobleaching (FRAP) experiments in hydrogels are an exceptionally accurate and fast, high-throughput method for characterizing solute self-diffusion within hydrogels.[4] Additionally, the confocal microscope used for FRAP can quantify the partitioning of the solutes into the hydrogel by comparing the concentrations of solutes within the hydrogel and in the source solution.

Solute diffusion and partitioning in hydrogels are generally understood to be affected by both the properties of the solute and properties of the hydrogel, but current models generalize the solute

contributions to their hydrodynamic radii and the hydrogel contributions to their swollen polymer volume fraction, mesh size, and fiber radius.[5-10] Our previous work investigating the diffusion of fluorescently tagged dextrans and linear poly(ethylene glycol) (PEG) in poly(vinyl alcohol) (PVA) hydrogels demonstrated that solute diffusivities in hydrogels do not scale consistently with hydrodynamic radius.[4] Dextran diffusivity in hydrogels decreased with increasing solute size, but PEG diffusivity increased with increasing solute size, indicating that solute interactions with the hydrogel based on shape or chemistry may disrupt the size-dependence of their diffusion within hydrogels.

In a theoretical analysis,[11] we argued that mesh size is a poor descriptor for solute diffusivity since it does not account for how the geometry of the swollen polymer network influences solute diffusivity. The proposed mesh radius correction for hydrogels with four, six, or eight chains converging at a junction aims to account for the limitations of using mesh size (Fig. 1). The accuracy of the mesh radius correction has not yet been experimentally tested, so we do so here. In addition to comparing our swollen polymer network (SPN) model predictions to measurements, we consider an alternative model, the large pore effective medium model (LPEM), which was derived by Liu et al. to account for hydrodynamic drag and network obstruction of solute diffusion only within accessible liquid-filled voids.[6] Liu et al. provide the complete algorithm for calculating solute diffusivities in hydrogels using the LPEM model in their work and demonstrate that it is more effective for representing the diffusivity of FITC-dextrans in hydroxyethyl methacrylate (HEMA)/methacrylic acid (MAA) hydrogels that then Ogston model,[12] Phillips model,[13] and effective medium model.[14, 15] The LPEM model notably uses obstruction/steric and hydrodynamic theories of solute diffusion in hydrogels[5, 6] and summarizes solute influence as the solute radius and hydrogel influences as the polymer volume fraction, network tortuosity, and the fiber radius (effectively ignoring the influences of the hydrogel structural parameters emphasized in the SPN model). Direct comparison between the predictions of the SPN and LPEM models is possible since both models use specific, quantitative parameters of the solute and network to predict the diffusion coefficient of the solute within the hydrogel, despite fundamental differences in how those values are calculated. Comparing theoretical models with robust experimental datasets is critical for evaluating the advantages and limitations of each model.

Additional design-relevant information about solute-hydrogel interactions can be gained by varying hydrogel structure using the independent, synthesis-controlled parameters considered in the SPN model.[7, 11] In our previous work, we investigated the diffusion of fluorescein, dextrans, and PEGs in eighteen PVA hydrogel formulations with varying initial polymer volume fraction (φ_0) and degree of polymerization between junctions (N_j). Here, we expand our focus on how hydrogel structure affects solute diffusivity and investigate solute partitioning with fluorescein and two sizes of dextrans in 73 formulations of multi-arm PEG hydrogels via simultaneous variation of four independent, synthesis-controlled structural parameters: initial polymer volume fraction, degree of polymerization between junctions, junction functionality (f), and frequency of chain-end defects (γ). Full-factorial analysis of how these structural parameters affect solute diffusion and partitioning in hydrogels provides unprecedented insight into how the hydrogel structure affects solute transport, including confirming possible interactions between structural parameters that might be obscured by a lower factorial matrix of formulations. Furthermore, the full factorial approach provides context on hydrogel structural design options by showing how the limitations of gelation depend on the intersection of multiple structural parameters.

In this study, we investigate the influences of hydrogel structure on solute diffusion and partitioning in hydrogels and evaluate correlations between hydrogel swelling, solute diffusion in hydrogels, and solute partitioning in hydrogels. We show that mesh size is an incomplete descriptor of solute transport in hydrogels, especially when considering junction functionality as a controllable parameter. Finally, we compare predictions of solute diffusion in hydrogels using the SPN model and the LPEM model. Coordinating fundamentally derived hydrogel modeling with robust experimental analysis clarifies the nuanced relationships between structure and function necessary for biomedically relevant hydrogel design.[16]

Methods

Norbornene-functionalization of hydroxyl-terminated multi-arm poly(ethylene glycol)

To create norbornene-functionalized multi-arm PEG precursors, hydroxyl-terminated multi-arm PEGs were functionalized based on adaptations of previously described protocols.[17, 18] Nine precursor polymers were used, all purchased from JenKem Technology USA (Plano, TX): (1) 4-arm, 10 kDa PEG, (2) 4-arm, 15 kDa, (3) 4-arm, 20 kDa, (4) 6-arm, 15 kDa, (5) 6-arm, 21 kDa, (6) 6-arm, 30 kDa, (7) 8-arm, 20 kDa, (8), 8-arm, 30 kDa, and (9) 8-arm, 40 kDa. The nine polymers were chosen to explore three junction functionalities (4, 6, and 8) and three sets of chain-arm lengths (approx. 2.5 kDa per arm, 3.75 kDa, and 5 kDa), which correspond to the degree of polymerization between junctions ($N_j = 115, 165, 215$). For all precursor macromers, polydispersity was confirmed by the manufacturer to be less than 1.05 and independently confirmed upon receipt by gel permeation chromatography (data available upon request). All other reagents and solvents were purchased from Sigma-Aldrich (St. Louis, MO) unless otherwise noted.

Briefly, all reagent concentrations were scaled to the expected concentration of hydroxyl end-groups for 5 g of the batch's PEG precursor. Initially, 5 molar equivalents (to PEG -OH groups) of N,N'-dicyclohexylcarbodiimide and 10 molar equivalents of 5-norbornene-2-carboxylic acid were mixed in 20 mL of dichloromethane under a nitrogen atmosphere and reacted at room temperature for 30 minutes. The product solution was then centrifuged at 3000 rpm for 10 minutes at room temperature in a Sorvall ST-16R centrifuge (Thermo Scientific, Waltham, MA) to separate the precipitated byproduct. The subnatant liquid was then added to a 40 mL dichloromethane solution on ice that contained 5 g of multi-arm PEG precursor, 5 molar equivalents of pyridine, and 0.5 molar equivalents of 4-(dimethylamino)pyridine (DMAP) under a nitrogen atmosphere. The resulting solution was left to react overnight on ice, under nitrogen, and in darkness. The reacted solution was precipitated and centrifuged twice in ice-cold diethyl ether, and the resulting pellet was left overnight to dry. The dry pellet was then resuspended in deionized water and dialyzed for 24 hours (2000 MWCO) before lyophilization and storage until use. Norbornene functionalization was confirmed via ^{1}H NMR (Agilent MN400) in triplicate with 16 scans per sample (other parameters set based on UT Austin NMR core facility standards).[19] Functionalization and NMR protocols are included in the supplementary materials.

Synthesis of multi-arm poly(ethylene glycol) hydrogels

Multi-arm PEG hydrogels were synthesized with simultaneous variation along four structural parameters. The structure of the multi-arm precursors defined the degree of polymerization between junctions ($N_j = 115, 165, 215$) and the junction functionality ($f = 4, 6, 8$). The concentration of the polymer in water defined the initial polymer volume fraction ($\varphi_0 =$

$0.050, 0.075, 0.100$), and the stoichiometric ratio of norbornene groups to crosslinking thiols (dithiothreitol, DTT) defined the frequency of chain-end defects ($\gamma = 0, 0.2, 0.4$). The combination of four structural parameters each with three values produced eighty-one unique hydrogel formulations, but six hydrogel formulations were not able to form stable gels (A4-N115-V050-F04, A4-N165-V050-F04, A4-N215-V050-F04, A4-N215-V075-F04, A4-N215-V100-F04, A8-N165-V050-F04) and two formulations were not synthesized due to limited resources (A6-N165-V050-F04, A6-N165-V075-F04), resulting in a total of 73 intact hydrogel formulations.

Briefly, multi-arm PEG solutions were made from 1X phosphate-buffered saline (PBS), one of the nine norbornene-terminated PEG precursors, DTT, and the photoinitiator Lithium phenyl-2,4,6-trimethylbenzoylphosphinate (LAP). Each solution was vortexed, then 3 mL of the solution was placed between glass plates with a 1.5 mm spacer and placed on a UV transilluminator (365 nm, 3 mW/cm^2; Analytik Jena, Germany) for 30 seconds on one side and 30 seconds on the other side. For each hydrogel formulation, photo-crosslinking was repeated with three different 3-mL solutions to account for variability. Immediately after photo-crosslinking, swelling was analyzed for each hydrogel formulation. Hydrogel synthesis protocols are included in the supplementary materials.

Volumetric swelling characterization

Volumetric swelling of the multi-arm PEG hydrogel formulations was characterized as previously described.[20] Briefly, the volumes of 18-mm diameter hydrogel disc samples were measured immediately following photo-crosslinking via a scale and density kit. Samples were then swollen to equilibrium for 24 hours and their volumes were measured again. Finally, samples were dried for 24 hours with heat (40 °C) and vacuum to measure the dry volumes. Swollen polymer volume fractions (φ_s) were calculated by dividing the dry volume by the swollen volume for each sample. Swollen polymer volume fractions were averaged for each hydrogel formulation ($n = 3$). Remaining hydrogel samples used for solute diffusivity and partitioning measurements were kept in the equilibrium-swollen state by storage in an excess of PBS.

Solute diffusivity characterization

The diffusivities of three solutes were determined in each of the 73 hydrogel formulations via FRAP as previously described.[4] In brief, fluorescein, fluorescein isothiocyanate-conjugated 4 kDa dextran (4 kDa FITC-Dextran), and 20 kDa FITC-dextran were selected as fluorescent solutes representing a range of solute sizes. Solute free diffusion coefficients (D_0) were determined via FRAP in solution experiments, and hydrodynamic radii (r_s) were calculated using the Stokes-Einstein equation, yielding 0.9 nm hydrodynamic radius for fluorescein, 1.7 nm for 4 kDa FITC-dextran, and 2.9 nm for 20 kDa FITC-dextran. For each solute and hydrogel formulation pairing, three hydrogel samples (2 mm diameter) were incubated for 24 hours in 3 mL of a 10 μM solution of the solute in PBS. 20 μM was used for 4 kDa FITC-dextran due to low fluorescence intensities at 10 μM. FRAP experiments were performed with three runs per sample ($n = 9$ per solute-formulation pairing) on a Zeiss LSM710 Confocal Microscope (Zeiss, Germany). FRAP analysis was performed using our high-throughput FRAP analysis MATLAB program,[4] yielding diffusion coefficients for each solute-hydrogel pairing. Solute diffusivity data and the FRAP experiment protocol are available online with links provided in the supplementary materials.

Solute partitioning characterization

For each solute-hydrogel pairing, solute partitioning into the hydrogel was measured by comparing fluorescence intensities. The pre-bleaching fluorescence intensity within each hydrogel and the fluorescence intensity of the source solution were measured under the same confocal imaging conditions (same experimental session, laser power, and intensity) using ImageJ analysis software. Measured intensities were compared to standard curves to confirm a linear relationship between intensity and concentrations, and then partitioning was calculated by the ratio C/C_0, where C is the solute concentration within the hydrogel and C_0 is the concentration in the source solution. Partition coefficients were averaged across the three scans per each of three samples per solute-formulation pairing ($n = 9$). Solute partitioning data is available online with links provided in the supplementary materials.

Predictive swollen polymer network modeling of solute diffusion in hydrogels

Structure-based predictions of mesh size, mesh radius, and specific solute diffusivities in each hydrogel were made using the SPN model.[7, 11] Swollen polymer volume fractions (φ_s) were calculated via Equation 1.

$$\varphi_s^{-\frac{1}{3}}\left[\ln(1-\varphi_s)+\varphi_s+\chi_1\varphi_s^2\right] = -1*\frac{\rho_d V_1}{M_r N_j}(1-\gamma)\left(1-\frac{2}{f}\right)\varphi_0^{\frac{2}{3}} \#(1)$$

In Equation 1, N_j, γ, f, and φ_0 are defined by the specific hydrogel formulation's network structure as explained above, and $\chi_1 = 0.426$ for PEG, $\rho_d = 1.12\ g/mL$ for PEG, $V_1 = 18\ mL/mol$ for water, and $M_r = 44\ g/mol$ for PEG.[20]

Mesh size (ξ) was calculated from the swollen polymer volume fraction, structural parameters, and identity constants using Equation 2, a modification of the Canal-Peppas equation.[7, 21]

$$\xi = \varphi_s^{-\frac{1}{3}}\left(\left(1-\frac{2}{f}\right)\bar{l}^2 C_\infty \lambda N_j\right)^{\frac{1}{2}} \#(2)$$

In Equation 2, $\bar{l} = 0.15\ nm$, $C_\infty = 4$, and $\lambda = 3$ for PEG.

Mesh radii (r_m) were calculated from mesh sizes and junction functionalities using Equation 3.[11]

$$r_m = \begin{cases} \frac{\sqrt{6}}{3}\xi & f = 4 \\ \frac{1}{2}\xi & f = 6 \\ \frac{\sqrt{2}}{4}\xi & f = 8 \end{cases} \#(3)$$

Solute diffusivities in hydrogels (D) were calculated according to Equation 4, a modified multiscale diffusion model based on hydrogel and solute properties.[4, 7, 11, 22]

$$\frac{D}{D_0} = \operatorname{erf}\left(\frac{r_{FVW}}{r_s}\right)\exp\left[-1*\left(\frac{r_s}{r_{FVW}}\right)^3\left(\frac{\varphi_s}{1-\varphi_s}\right)\right] + \operatorname{erfc}\left(\frac{r_{FVW}}{r_s}\right)\exp\left[-\frac{\pi}{4}\left(\frac{r_s+r_f}{r_m}\right)^2\right] \#(4)$$

In Equation 4, D_0 is the diffusivity of the solute in a free aqueous solution and r_s is the associated hydrodynamic radius of the solute. As measured previously,[4] for fluorescein, $D_0 = 278\ \mu m^2/s$ and $r_s = 0.88\ nm$. For 4 kDa FITC-dextran, $D_0 = 142\ \mu m^2/s$ and $r_s = 1.73\ nm$. For 20 kDa FITC-dextran, $D_0 = 85\ \mu m^2/s$ and $r_s = 2.89\ nm$. The average radius of free volume voids in water is $r_{FVW} = 0.269\ nm$,[22] and the fiber radius of PEG with a monolayer of water is $r_f = 0.51\ nm$.

The primary method for predicting solute diffusivity in hydrogels used in this work is to calculate Equations 1-4 in sequence with D as the output. To compare with prior models that ignored how mesh radius differs from mesh size based on network geometry, diffusion coefficients for each solute and hydrogel pairing were also calculated with Equation 3 omitted and with half the mesh size ($\xi/2$) substituted for mesh radius in Equation 4 (reproducing the multiscale diffusion model of Axpe et al.[22] without the mesh radius correction).[11] SPN model predictions are available online with links provided in the supplementary materials.

Predictive large pore effective medium modeling of solute diffusion in hydrogels

Solute diffusivities in hydrogels were calculated using the LPEM model[6] as an external comparison to the swollen polymer network model predictions. The full derivation of the LPEM model is provided in the original work.[6] Here, we repeat the LPEM predictive calculations for multi-arm PEG hydrogels, using 0.51 nm as the fiber radius for PEG,[22] a tortuosity of 1 for dilute PEG hydrogels,[23] and the measured swollen polymer volume fractions as the relevant polymer volume fractions. LPEM model predictions and the R script used to make them are available online with links provided in the supplementary materials.

Results

Experimental design and hydrogel synthesis

This work aims to experimentally validate the fundamental model-predicted relationships between hydrogel structure and solute transport in hydrogels, specifically focusing on the diffusion coefficients and partitioning of solutes in the hydrogels. A library of 73 unique multi-arm PEG hydrogel formulations was synthesized by systematic, simultaneous variation of four structural parameters: the degree of polymerization between junctions (N_j), the junction functionality (f), the initial polymer volume fraction (φ_0), and the frequency of chain-end defects (γ).[11] Six of the initially planned 81 formulations did not form stable, intact hydrogels, and two were not synthesized due to limited synthesis materials. Of the six incomplete formulations, all six had the highest frequency of chain-end defects ($\gamma = 0.4$), five had four arms ($f = 4$), and four had the lowest initial polymer volume fraction ($\varphi_0 = 0.050$). Since no one parameter value consistently failed to form intact hydrogel formulations, this suggests that gelation is affected by the combination of all four structural parameters. Notably, the lowest frequency of chain-end defects ($\gamma = 0.4$) was chosen to be just above the required "real" junction functionality of >2 for the four-arm precursors. Two connecting chains or less from each macromer would result in a linear polymer or no polymerization, respectively. That four of the four-arm, $\gamma = 0.4$ formulations formed intact hydrogels near this boundary of the gelation space indicates that the photoinitiated norbornene-DTT crosslinking reaction is robust and efficient, despite the likelihood of other unmeasured variations in the overall network structure of each hydrogel formulation. Comparison with other methods of crosslinking multi-arm PEG hydrogels may help to clarify the role of crosslinking reactions on overall network structure.[18, 24-27]

Each hydrogel formulation was paired with three solutes of varying sizes for diffusion and partitioning experiments. Fluorescein (0.9 nm hydrodynamic radius) represents a small, soluble molecule, and 4 kDa and 20 kDa FITC-dextran (1.7 nm and 2.9 nm) are included to show how increasing solute size affects their transport in hydrogels. Diffusivity and partitioning were measured directly for each solute-hydrogel pairing and compared to fundamental predictions made using the SPN and LPEM models.[4, 6, 7, 11]

Main solute size effects on partitioning and diffusion

Generally, solute diffusivity within hydrogels and partitioning into hydrogels decreased with increasing solute size (Fig. 2). The hydrogel formulation-dependent ranges for solute diffusivity and partitioning per solute were broadest for the smallest solute, fluorescein, and narrowest for the largest solute, 20 kDa FITC-dextran. Notably, some of the fluorescein-hydrogel pairings exhibited diffusion coefficients higher than the measured diffusion coefficient of fluorescein in free solution (278 $\mu m^2/s$). This is likely due to fluorescein forming dimers in free solution, whereas the more constrained hydrogel environment would favor monomers that are smaller and diffuse more quickly (estimated $D_0 = 489\ \mu m^2/s$ and $r_s = 0.50\ nm$).[4] 4 kDa and 20 kDa FITC-dextrans in hydrogels all have diffusivities lower than their diffusivities in free solution (142 $\mu m^2/s$ and 85 $\mu m^2/s$).

The partition coefficients much greater than one for the fluorescein-hydrogel pairings indicate that fluorescein has an attractive chemical interaction with the PEG hydrogels, likely resulting from the negative charge of fluorescein, which is not shared by the neutral FITC-dextrans. The widely spread, multimodal distribution of partition coefficients for fluorescein in the hydrogels, including partition coefficients less than one, indicates that the network structure has a significant effect on fluorescein partitioning. 4 kDa FITC-dextrans have partition coefficients slightly greater than one in three hydrogel formulations but are otherwise less than one, and all 20 kDa FITC-dextran pairings have partition coefficients well below one.

Unlike diffusivity, which is measured by self-diffusion coefficients within hydrogels, partitioning is affected by the surface accumulation of solutes. Surface accumulation is more likely for larger solutes that can be excluded from the network, as shown by qualitative imaging at the edges of hydrogel samples (Supp. Fig. S1). Negligible surface accumulation was observed for fluorescein (Supp. Fig. S1A), and significant accumulation was observed for the larger 20 kDa FITC-dextran (Supp. Fig. S1B), which may block solute transport into the network and contribute to the reduced large-solute partitioning into hydrogels. Notably, none of the 73 hydrogel formulations completely excluded any of the three solutes.

Hydrogel structure effects on partitioning and diffusion

The 73 multi-arm PEG hydrogel formulations based on a matrix of four structural parameters provide a robust dataset for evaluating how hydrogel structure affects the partitioning and diffusion of solutes in hydrogels. Comparing swollen polymer volume fractions to solute diffusion and partitioning, grouped by degree of polymerization between junctions (Fig. 3), shows that solute diffusivity tends to decrease with increasing swollen polymer volume fraction (Fig. 3A-C), whereas partitioning does not show a consistent overall trend (Fig. 3D-F). Curiously, for fluorescein and 20 kDa FITC-dextran, swelling-diffusivity trends are separated by degree of polymerization between junctions, with increasing degrees shifting the trend down and to the left (Fig. 3A,C) but the intermediate size solute, 4 kDa FITC-dextran does not show the same dependence on the degree

of polymerization between junctions (Fig. 3B). Though not further separated by color and shape, initial polymer volume fraction, junction functionality, and frequency of chain-end defects have redundant effects on the relationship between swelling and solute diffusivity (see Supp. Fig. S2). Increasing initial polymer volume fraction and junction functionality decreases diffusivity and increases swollen polymer volume fraction, and increasing the frequency of chain-end defects increases diffusivity and decreases the swollen polymer volume fraction.

Contrasting the strongly correlated diffusivity trends, solute partitioning into the hydrogels inconsistently correlates with swollen polymer volume fraction and the four controlled structural parameters. For 20 kDa FITC-dextran, partitioning appears to decrease with increasing swollen polymer volume fraction (Fig. 3F), which would seem reasonable on the assumption that having more polymer would reduce the solute-accessible volume within the hydrogel, but fluorescein and 4 kDa FITC-dextran do not match this trend (Fig. 3D-E). Furthermore, the grouping effect of the degree of polymerization between junctions is not consistent across the three solutes, and the degree of polymerization between junctions does not have a consistent influence on partitioning.

Summarizing the main effects of structural parameters on diffusion and partitioning is informative to hydrogel design (Table 1). Generally, initial polymer volume fraction and junction functionality have simple interactions with solute diffusivity and partitioning. Increasing either structural parameter consistently decreases both diffusivity and partitioning.

Increasing the frequency of chain-end defects increases diffusivity across all three solutes but has a size-dependent effect on partitioning. Increasing the frequency of chain-end defects decreases partitioning for the small solute, fluorescein, has little effect on the mid-sized solute, 4 kDa FITC-dextran, and increases partitioning for the largest solute, 20 kDa FITC-dextran. This size-dependent shift in partitioning, especially in the context of a consistent diffusivity effect, establishes the frequency of chain-end defects as a potential high-contrast parameter for hydrogel-based separations applications.

As indicated in Fig. 3, the degree of polymerization between junctions has an inconsistent effect on solute diffusivity and partitioning. No trends were conserved across the three solutes for either diffusivity or partitioning. These results starkly contrast both modeling predictions and prior data with similar structural manipulations on comparable hydrogel systems,[4, 7, 11, 20] as will be further discussed in the following sections.

Relationship between solute partitioning and diffusion in hydrogels

Solute diffusivity and partitioning are both key properties of solute transport in hydrogels, but they are not correlated across variations in multiple structural parameters and varying solute sizes (Fig. 4). However, according to the relationships in Table 1, if initial polymer volume fraction and junction functionality were the only two structural parameters varied, they would be positively correlated. This difference demonstrates how limited experimental spaces can lead to oversimplified conclusions about structure and property interactions.

Mesh size, mesh radius, and network geometry

Mesh size is often used as an intermediate structural parameter to summarize solute transport in hydrogels.[28-35] Unlike the four structural parameters used to define hydrogel formulations throughout this work, mesh size is an intermediate descriptor because it is a composite result of several network interactions and therefore not independently tunable. It has not been measured

directly because it is a nanoscale, average property that must be measured in a hydrated state. Moreover, the novel ability to explicitly control junction functionality with multi-arm PEG hydrogels requires that we consider network geometry in addition to mesh size when evaluating solute transport in hydrogels.[11] We previously suggested that mesh radius should replace mesh size in the multiscale diffusivity model (as shown in Eq. 4), but we did not have experimental data on hydrogels with varying junction functionality to prove our theoretical argument at the time.

Selecting a subset of hydrogel formulations that only varies junction functionality ($f = 4,6,8$) while keeping the other structural parameters consistent ($\varphi_0 = 0.075, N_j = 165, \gamma = 0.2$), we observe that diffusivity predictions based on mesh radius better correlate with measured values than predictions based solely on mesh size (Fig. 5). For fluorescein, both mesh size- and mesh radius-based predictions positively correlated with measured diffusivities (Fig. 5A), but for the larger 4 kDa FITC-dextran and 20 kDa FITC-dextran, mesh-size based predictions negatively correlated with measured diffusivities (Fig. 5B-C). With larger solutes that are closer in size to the mesh radius and mesh size of the network, the effect of network geometry on solute diffusivity is more substantial. The junction functionality-dependent shift from negative prediction-measurement correlation using the mesh size equation to positive prediction-measurement correlation using the mesh radius equation is consistent across the full library of hydrogel formulations (Supp. Fig. S4). These results indicate that mesh size is insufficient for predicting the diffusivity of larger solutes in hydrogels without addressing network geometry via the mesh radius correction.[11]

Comparison with the Large Pore Effective Medium Model

The SPN model is one of several models under active investigation for solute transport in hydrogels.[5] Many of these models, including the SPN model, have not been experimentally cross-evaluated by research groups other than the ones who proposed them, meaning that they are often tested on limited datasets. One of the main restrictions to these cross-evaluating studies is that researchers do not provide enough information about the models or the raw experimental datasets they are interpreting with the models to facilitate comparisons. Serious, unbiased cross-evaluation efforts would help to identify the advantages and limitations of different models. Here, we consider the LPEM model proposed by Liu et al.[6] because 1) it derives from obstruction and hydrodynamic theories, complementing the obstruction and free volume theory sources for the SPN model, 2) Liu et al. demonstrated that it describes the diffusion of 4 kDa FITC-dextran and 20 kDa FITC-dextran in HEMA/MAA hydrogels better than three related models, 3) it is presented with fully defined equations so the calculations can be applied to a different dataset, and 4) it is a fundamental model with no phenomenological fitting parameters. However, like other existing models, it neglects the influence of network geometry on solute transport within hydrogels, instead assuming a random distribution of network chains, extending from obstruction theory and the Ogston model.

For the multi-arm PEG hydrogels, the LPEM model predictions became less accurate than the SPN model for larger solutes (Fig. 6). For fluorescein, the LPEM-predicted diffusivity increased with the increasing degree of polymerization between junctions like the SPN model's predictions despite the measured diffusivity decreasing (Fig. 6A,D). The consistent false correlation for both the LPEM model and SPN model supports our hypothesis that the measured relationship between the degree of polymerization between junctions and solute diffusivity in multi-arm PEG hydrogels indicates a novel mechanism of structure-property interactions in hydrogels. For 4 kDa and 20 kDa FITC-dextran, the LPEM model predictions deviate from measurements at low diffusion coefficient values whereas the SPN model predictions maintain a positive correlation for all

structural parameters other than the degree of polymerization between junctions. For larger solutes, the SPN model better accounts for the influences of hydrogel structure on solute transport than the LPEM model does.

Discussion

Network structure affects solute diffusivity in PEG and PVA hydrogels

With a robust library of multi-arm PEG hydrogels, we identified how four independent structural parameters of hydrogel design ($N_j, f, \varphi_0, \gamma$) affect solute self-diffusion within hydrogels and partitioning into hydrogels. Notably, junction functionality, initial polymer volume fraction, and frequency of chain-end defects have consistent and model-predictable effects on solute diffusivities, but the degree of polymerization between junctions has an inconsistent, unpredicted effect. Not only was the influence of the degree of polymerization on solute diffusivities different depending on the solute (Table 1), but the measured relationships differed from predictions (Fig. 6A-C). This result sharply contrasts our recent study of solute transport in PVA hydrogels using the same FRAP experiments and analysis method.[4] In the PVA hydrogels, initial polymer volume fraction and degree of polymerization between junctions were independently manipulated and the diffusivities of fluorescein, 4kDa FITC-dextran, and 20 kDa FITC-dextran as well as other solutes were measured in each hydrogel formulation. With PVA hydrogels, increasing initial polymer volume fraction decreased diffusivities for all solutes as predicted and as measured here, but increasing the degree of polymerization between junctions consistently increased diffusivity as predicted, unlike with the multi-arm PEG hydrogels in this study. Future work should investigate whether the unexpected effects of the degree of polymerization between junctions on solute transport for multi-arm PEG hydrogels reproducibly apply to a broader variety of solutes. Because the effect was shown here for a large, redundant library of hydrogel formulations, we hypothesize that there is a substantial, unanticipated mechanism relating the degree of polymerization between junctions to solute diffusivities for multi-arm PEG hydrogels.

Mesh radius captures junction functionality effects on solute transport

This study of solute transport in hydrogels definitively demonstrates that including mesh radius in the modeling of solute transport in hydrogels is an improvement over mesh size-based models. The conversion from mesh size to mesh radius primarily addresses how changing junction functionality affects the molecular geometry of a swollen polymer network.[11] This work extends prior work by Lutolf and Hubbell[36] and Lee, Tong, and Yang[28, 29] to understand how changing junction functionality affects solute transport in hydrogels. However, Lutolf and Hubbell did not directly measure solute transport in hydrogels,[36] and Lee, Tong, and Yang interpreted changes in solute diffusivity as a function of junction functionality (with equivalent mesh sizes) to be the result of changing network homogeneity.[28, 29] The introduction of mesh radius and consideration of network geometry provides a predictable fundamental mechanism for their experimental results.

Solute transport properties in hydrogels are not universally correlated

Lutolf and Hubbell created multi-arm PEG hydrogels with different junction functionalities but used swelling ratios as a proxy for solute transport properties.[36] Similarly, Cha et al. effectively varied the frequency of chain-end defects in PEG diacrylate hydrogels but similarly assumed that the swelling ratio summarizes solute transport properties.[37] Here we show in Fig. 3 that swelling is not universally correlated with solute diffusivity or partitioning in hydrogels (noting that the swelling ratio is the inverse of the swollen polymer volume fraction). This work therefore demonstrates that

assuming swelling ratios can be used as proxies for other solute transport properties is overly simplistic and inappropriate. Instead, relevant solute transport properties should be measured directly where possible—for example, the FRAP-based self-diffusion of solutes within hydrogels measured here is not guaranteed to correspond to the diffusion coefficients of solute release from hydrogels.

Similarly, this work disproves the assumption that mesh size or even mesh radius can be used to summarize a hydrogel's solute transport properties. Neither mesh size nor mesh radius completely captured the differences in solute diffusivity or partitioning between different hydrogel formulations. Even once used to predict solute diffusivities with the SPN model, which also scales based on the swollen polymer volume fraction, there were systematic discrepancies between the prediction and the measured diffusivities. Since different solute transport properties are shown here to not be correlated, it may be impossible to identify a single hydrogel formulation-specific parameter that summarizes how the hydrogel influences solute transport.

Browning et al.[30] and Munoz-Pinto et al.[38] both summarized what they described as diffusion experiments using mesh size. However, they performed partition coefficient measurements, where solutes diffused into the hydrogels over 24 hours and then were released into a second solution for 24 hours. They compared the concentration of solutes in the initial and final solutions, effectively yielding a partition coefficient instead of a diffusion coefficient, which was unclear in their figures due to their use of mesh sizes. We showed in Fig. 4 that partition coefficients and diffusion coefficients are not robustly correlated within hydrogels. The absence of correlations for solute transport properties in hydrogels indicate the need for more extensive experimental study and modeling of solute transport properties hydrogels with a focus on matching the measured property to the target application.

Solute size-based models oversimplify solute-hydrogel interactions

The modified multiscale diffusion model used in this study maintains the assumption that solute diffusion in hydrogels scales universally with solute size. We demonstrated the limitations of this assumption in our previous study of FITC-dextrans and FITC-PEGs diffusing in PVA hydrogels.[4] Preliminary studies with the multi-arm PEG hydrogels showed that FITC-PEGs partitioned homogeneously into the PEG-based hydrogels, but their self-diffusion was extremely slow compared to the diffusion of FITC-dextrans in the PEG hydrogels or either solute group in PVA hydrogels (data not shown), so we concluded that there is a specific PEG-PEG interaction and only used FITC-dextrans for the full study. Furthermore, the 70 kDa FITC-dextrans used in the PVA study were partitioned into the multi-arm PEG hydrogels at such low concentrations that we were unable to measure their diffusion coefficients. Successfully including the 70 kDa FITC-dextrans would have enabled a study of size effects in chemically similar molecules without the confounding chemical differences between fluorescein and FITC-dextrans, potentially clarifying whether the 4 kDa FITC-dextran behavior was anomalous as suggested by the fluorescein and 20 kDa FITC-dextran data or part of a scaling relationship specific to FITC-dextrans.

Identifying the conditions for size-based equivalency of solute diffusion in hydrogels is critical for drug and protein delivery applications. Here, as in many comparable studies,[39-41] we use FITC-dextrans as readily available, globular, hydrophilic solutes that cover a range of sizes relevant to bioactive soluble proteins (~1-10 nm hydrodynamic radius). However, shape, charge, and solute-hydrogel interaction differences may mean that these solutes are poor substitutes for the proteins they aim to model. A positive proof-of-concept study by Rehmann et al. indicated that two proteins

of near-equivalent hydrodynamic radii (Bovine serum albumin at 7.2 nm and platelet-derived growth factor-BB at 7.0 nm) have similar release profiles from the same hydrogel formulation, suggesting that some extent of size-diffusivity equivalence is viable.[32] The confounding effects of shape, charge, and other solute-hydrogel interactions are under-investigated, and the high-throughput FRAP experiments and analysis here could help to clarify their nuanced effects.

Surface accumulation of solutes may affect partitioning and diffusivity

This study focuses on the self-diffusion of solutes within a hydrogel as measured by FRAP, and the partitioning is likewise measured based on the solute concentration within the hydrogels as measured by confocal microscopy. Alternatively, it is common to characterize solute diffusion from hydrogels via release studies[28] and measure partitioning based solely on changes in supernatant concentrations.[30] The greatest difference between these methods is the effect of solute accumulation at the surface of the hydrogel. In release studies, surface accumulation contributes to burst release, and measuring partition coefficients via supernatant concentrations does not distinguish between surface accumulation and partitioning into the interior of the hydrogel, reducing accuracy and reproducibility. In this work, the self-diffusion of solutes is measured within hydrogels via FRAP, and partition coefficients are based on the interior concentration of solutes, avoiding the experimental limitations of prior diffusion and partitioning methods.

The confocal microscopy used for FRAP experiments facilitated qualitative imaging of solute surface accumulation on the edges of hydrogel samples (Supp. Fig. S1). The surface accumulation may also affect FRAP experiments by screening larger solutes but allowing smaller solutes into the hydrogel. Since the FITC-dextrans have a distribution of solute sizes, the distribution that made it into the hydrogel may be different from the distribution in the solution, effectively distorting model predictions based on the average solute size in solution. Future studies should measure whether the partitioning of polydisperse solutes into hydrogels favors the smaller solutes, especially where there is significant surface accumulation. Such distribution shifts could explain the discrepancies observed between 4 kDa and 20 kDa FITC-dextrans.

Study limitations

Practical limitations of this study include the small number of solutes studied (3) compared to our previous study with seven solutes,[4] some technical limitations with the confocal microscope, and the lack of a complete predictive model for solute partitioning in hydrogels. As discussed above, FITC-PEG solutes diffused slowly in the multi-arm PEG hydrogels, likely due to specific PEG-PEG interactions. With more time and experimental optimization, it would be informative to measure the diffusion coefficients of those FITC-PEGs in the multi-arm PEG hydrogels, but the slow diffusion means that those studies will take much longer than the FITC-dextran diffusion studies. Additional studies with fluorescent probes other than fluorescein may reveal biases associated with that probe, and protein transport in hydrogels should be studied for further analysis of solute shape, chemical interactions with the network, and biological relevance.[32, 42] Also, the six degrees of polymerization between junctions studied in the PVA hydrogel study generated a continuous response trend,[4] whereas only three values for each structural parameter were used in this study, meaning that little could be concluded from data that did not produce a continuous trend over the three values (e.g., for the degree of polymerization between junctions). Practically, the need for a higher, 20 μM concentration of 4 kDa FITC-dextran introduced the possibility of concentration-dependent behavior, which was not thoroughly studied here.

Additionally, midway through the FRAP experiments for this study, maintenance was performed on the confocal microscope that greatly increased the laser power, possibly creating a measurement artifact dividing data before and after the increase. To help mitigate this distortion, laser powers and gains were selected that kept scans within the linear intensity-concentration ranges, and standard curves were taken at each laser power and gain used.

A robust predictive model for solute partitioning in hydrogels would allow more hypothesis-driven experimentation on solute partitioning in hydrogels and facilitate the sort of iterative model refinement we demonstrated with solute diffusion modeling in Fig. 5 and Fig. 6. Kotsmar et al. predicted partitioning of solutes into hydrogels based on the integration of the Ogston model,[39] but it is unclear if a similar model could be developed that is consistent with the current iteration of the SPN model, which incorporates features of free volume theory as well as the Ogston-based obstruction theory.[7] It would also be worthwhile to investigate a greater variety of models for solute transport in hydrogels, as was demonstrated here with the LPEM model.[5] Ultimately, fundamentally derived, experimentally validated models of solute transport in hydrogels should be able to account for the nuances of solute release, partitioning, and self-diffusion within hydrogels. Comprehensive models of solute transport in hydrogels will only be possible with continuous, iterative modeling and experimentation using a broad variety of solutes and hydrogel formulations.

Conclusions

In this contribution, we demonstrate that solute diffusion and partitioning in hydrogels are both linked to the hydrogel's network structure, but they are not always correlated. Notably, the frequency of chain-end defects has a discerning effect on diffusivity and solute partitioning. A higher frequency of chain-end defects consistently increased diffusivity but shifted from decreasing to increasing partitioning with increasing solute size.

Multi-arm PEG hydrogels have exceptional control of junction functionalities based on the number of arms per precursor molecule, allowing precise investigation of how junction functionality affects solute transport. The experimental results confirmed our theory that more geometrically restrictive networks reduce solute diffusivity even with equivalent mesh sizes. We therefore recommend the use of mesh radius over mesh size in models relating hydrogel structure to solute diffusivity.

FRAP and confocal-based partitioning methods overcome some of the problems associated with surface accumulation during solute transport in hydrogel studies. However, large polydisperse solutes may still create a screening effect in these studies where only the smaller solutes make it into the hydrogels. This effect should be investigated in future studies.

Overall, complementary FRAP and partitioning experiments enable robust, high-throughput studies of solute transport in hydrogels that can provide overwhelming evidence for questions unanswered by smaller-scale or unidimensional studies (e.g., only varying solute size). Further use of these methods, especially when used to test assumptions in fundamental hydrogel models, will accelerate predictive hydrogel design for diverse biomedical applications. As shown by the differences between predicted and measured diffusivities in this work, there is still much room for improving hydrogel design models, even with the relatively simple multi-arm PEG hydrogels and solute transport properties. Thoroughly validated, accurate models are required for the clinically relevant scale-up of precise and highly tunable hydrogel scaffolds and drug delivery devices.

Conflicts of Interest

There are no conflicts of interest to declare.

Acknowledgments

Support for this work was provided by the National Science Foundation (1610403 for N.R.R.) and the National Institutes of Health (EB022025, GM043337 for N.A.P.). N.A.P. is further supported by the Cockrell Family Regents Chair in Engineering for the Institute of Biomaterials, Drug Delivery, and Regenerative Medicine and the UT-Portugal Collaborative Research Program. N.R.R. is further supported by the Cockrell Graduate Continuing Fellowship. We thank Professor Nathaniel Lynd and Benjamin Pedretti at UT Austin for performing GPC to confirm the molecular weight and dispersity of our multi-arm PEG precursors as well as Garrett Blake and the UT Austin NMR core facility for training and support on ^{1}H-NMR studies.

552 **Figures**

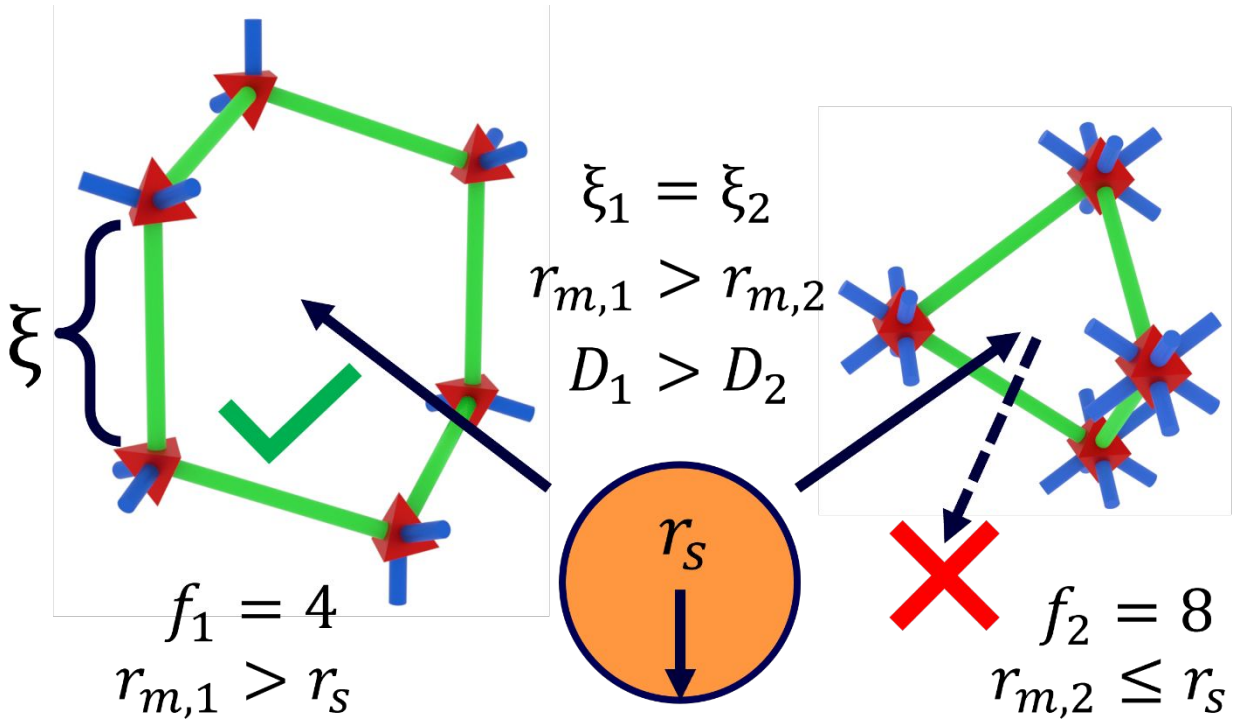

553

554 **Figure 1. Model predictions of how network geometry affects solute transport in hydrogels.**
555 For two network portals with equivalent mesh sizes (ξ) but different junction functionalities ($f = 4,8$
556) and therefore different mesh radii (r_m), a large solute (with radius r_s) may be able to pass more
557 easily through the portal with the lower junction functionality (higher mesh radius) than the portal
558 with the higher junction functionality (and lower mesh radius). Resultingly, diffusion coefficients (D
559) are higher in the network with a higher mesh radius. Network chains are represented as straight
560 rods for clarity, and the smallest network portal for each junction functionality is highlighted in
561 green.

562

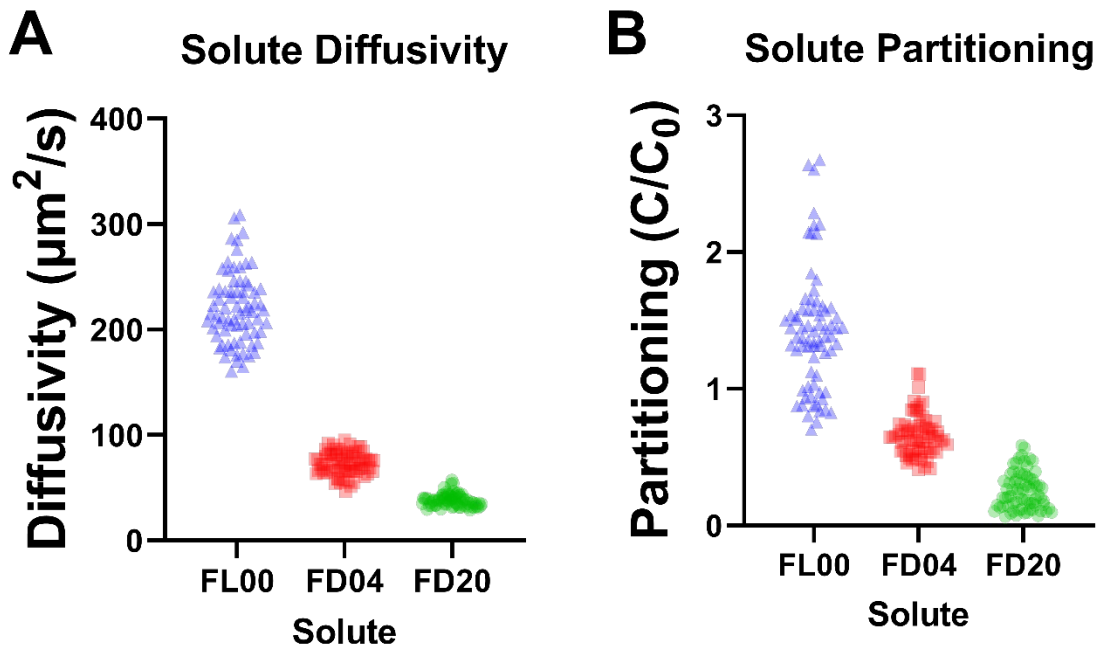

Figure 2. Solute diffusivity (A) and partitioning (B) in multi-arm PEG hydrogels. FL00 is fluorescein (0.9 nm hydrodynamic radius), FD04 is 4 kDa FITC-dextran (1.7 nm), and FD20 is 20 kDa FITC-dextran (2.9 nm). Each point represents a unique solute-hydrogel formulation pairing. Error bars are not shown for visual clarity.

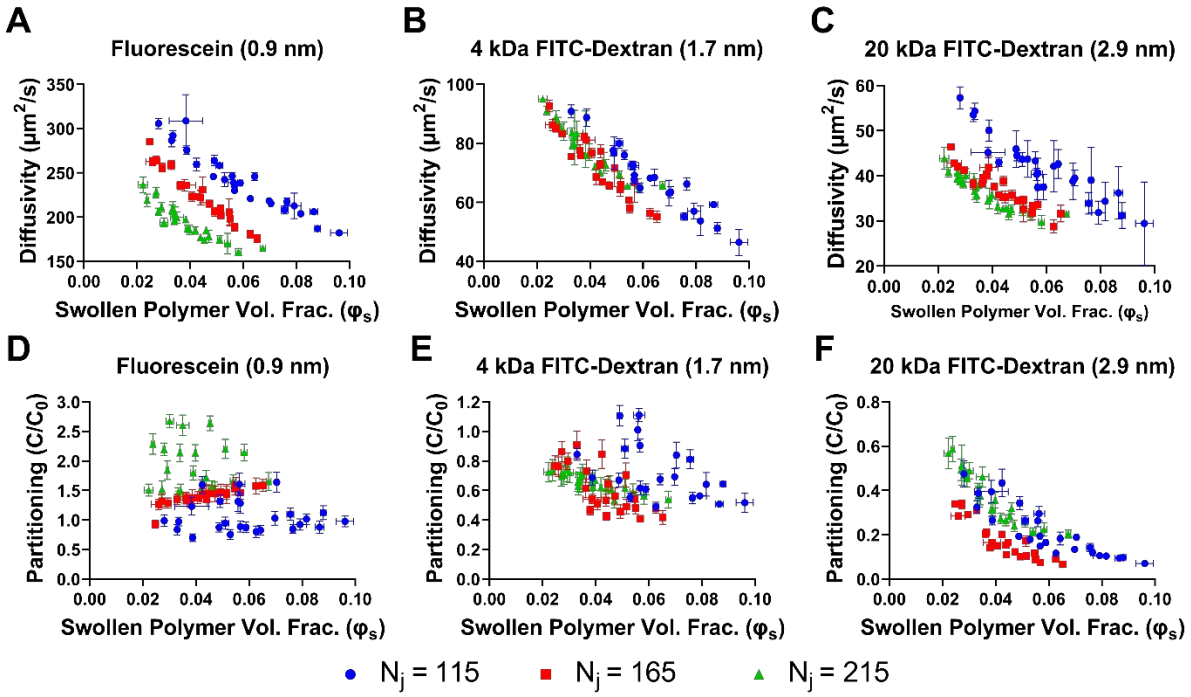

Figure 3. The influence of the degree of polymerization between junctions (N_j) on (A-C) the relationship between swelling and diffusivity and (D-F) between swelling and partitioning in multi-arm PEG hydrogels. Whereas the other three structural parameters studied have an overlapping effect on the relationship between swelling and diffusivity, N_j has the distinctive effect of higher values decreasing both swollen polymer volume fraction and diffusivity, at least for fluorescein (A) and 20 kDa FITC-dextran (C). However, swelling-partitioning trends are inconsistent across formulation and solute. Error bars represent standard deviations (for swelling, $n = 3$, for diffusivity and partitioning, $n = 9$).

579 **Table 1. Hydrogel Structural Parameters Main Effects on Diffusivity and Partitioning**

Structural Parameters	Fluorescein (0.9 nm)	4 kDa FITC-Dextran (1.7 nm)	20 kDa FITC-Dextran (2.9 nm)
Initial Polymer Volume Fraction (φ_0)	D↓, P~	D↓, P↓	D↓, P↓
Degree of Polymerization Between Junctions (N_j)	D↓, P↑	D↑, P↓*	D↓, P↑*
Junction Functionality (f)	D↓, P↓*	D↓, P↓	D↓, P↓
Frequency of Chain-End Defects (γ)	D↑, P↓	D↑, P~	D↑, P↑

580 D for diffusivity, P for partitioning, ↑ indicates a property increase when the parameter increases,
581 ↓ indicates the property decreases when the parameter increases. * indicates that the trend is
582 not consistent across formulations, and ~ indicates that the parameter appears to not affect the
583 property. An example of the figures used to evaluate these relationships is provided in Supp.
584 Fig. S3.

585

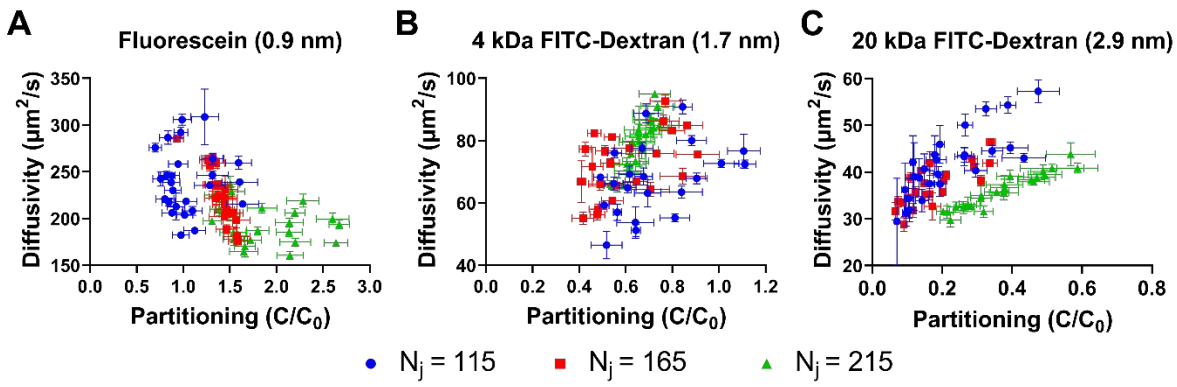

Figure 4. Relationship between diffusivity and partitioning in multi-arm PEG hydrogels. Trends were ambiguous across solutes and hydrogel structural parameters. Overall, there is not a strong or structurally consistent correlation between solute diffusivity and partitioning. Error bars represent standard deviations ($n = 9$).

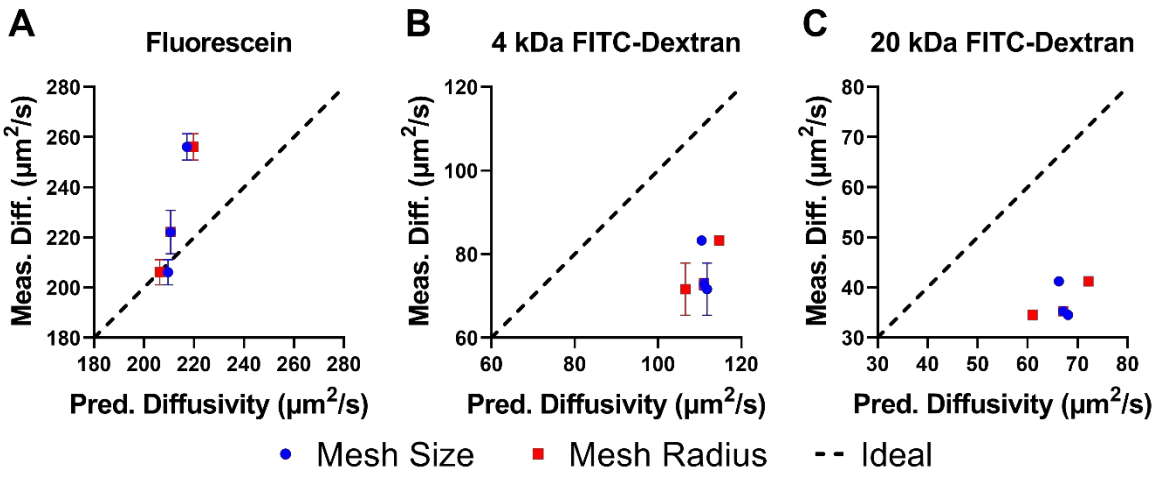

Figure 5. Comparing mesh size-based predictions and mesh radius-based predictions to measured diffusivities for a subset of hydrogel formulations with changing junction functionality. Three hydrogel formulations with changing junction functionality ($f = 4,6,8$) and other structural parameters held constant ($\varphi_0 = 0.075, N_j = 165, \gamma = 0.2$) were used to summarize how junction functionality affects predictions of solute diffusivity in hydrogels. Mesh radius predictions positively correlate with measurements, whereas mesh size-based predictions negatively correlate with measurements for larger solutes (B,C). A comparison for all hydrogel formulations is provided in Supplementary Figure S3. Error bars represent standard deviations ($n = 9$). Ideal: 1:1 correlation between prediction and measurement.

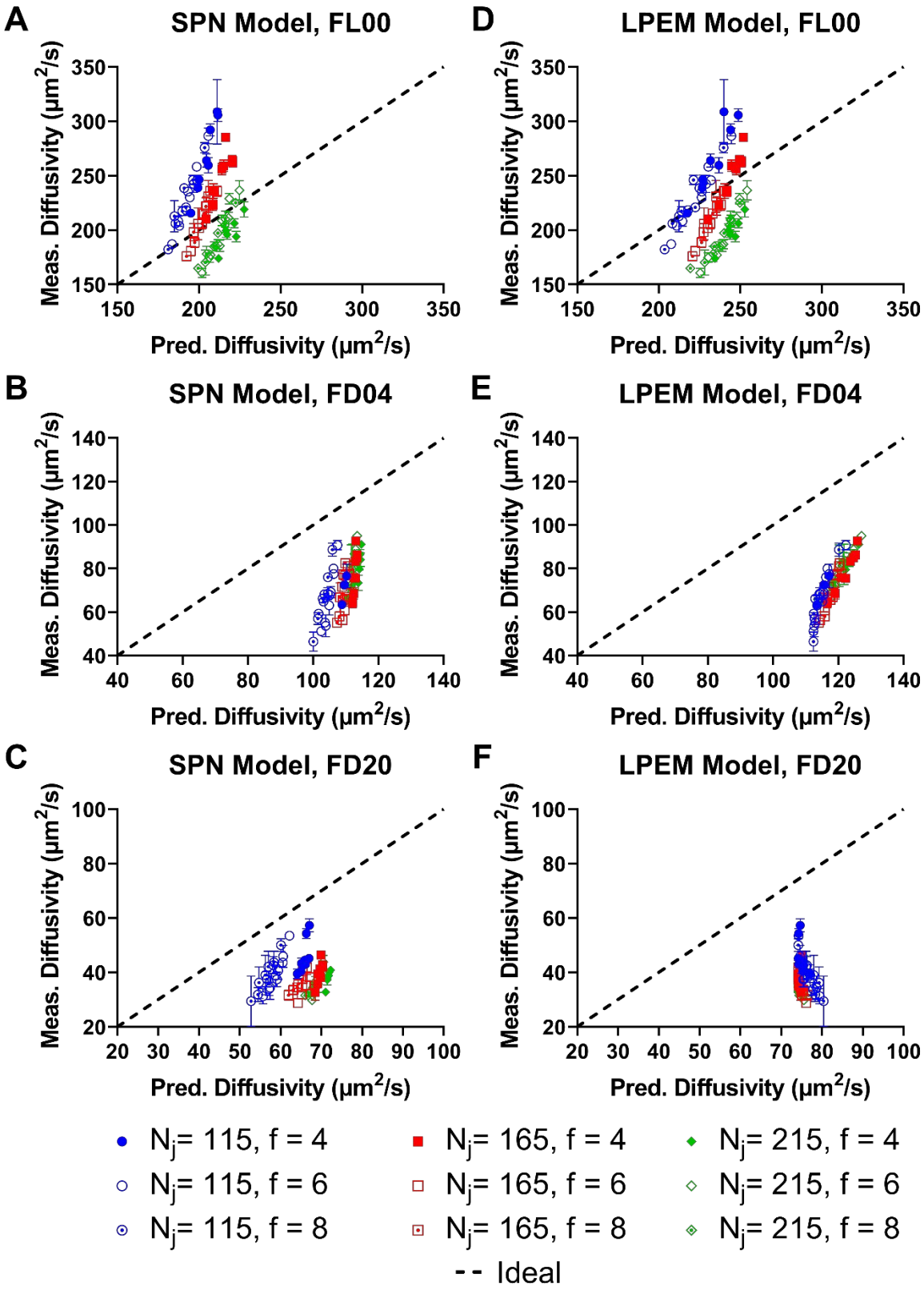
A
SPN Model, FL00
D
LPEM Model, FL00
B
SPN Model, FD04
E
LPEM Model, FD04
C
SPN Model, FD20
F
LPEM Model, FD20
Meas. Diffusivity (μm²/s)
Pred. Diffusivity (μm²/s)
Nj= 115, f = 4
Nj= 165, f = 4
Nj= 215, f = 4
Nj= 115, f = 6
Nj= 165, f = 6
Nj= 215, f = 6
Nj= 115, f = 8
Nj= 165, f = 8
Nj= 215, f = 8
Ideal

604

Figure 6. The swollen polymer network (SPN) model predictions vs. the large pore effective medium (LPEM) model predictions compared to measured values. (A-C) the swollen polymer network model explicitly addresses the influence of hydrogel structural parameters and uses free volume theory to account for large solutes, whereas (D-F) the large pore effective medium model is based on obstruction and hydrodynamic theories and inaccurately predicts how hydrogel structure affects solute diffusivity at high solute sizes. (A,D) Both models inaccurately predict the influence of the degree of polymerization between junctions (N_j) on fluorescein diffusivity. Error bars represent standard deviations ($n = 9$). FL00: fluorescein, 0.9 nm hydrodynamic radius. FD04: 4 kDa FITC-dextran, 1.7 nm. FD20: 20 kDa FITC-dextran, 2.9 nm. Ideal: 1:1 correlation between prediction and measurement.

References

1. J. J. Kim and K. Park, *Bioseparation*, 1998, **7**, 177-184.
2. J. Li and D. J. Mooney, *Nat Rev Mater*, 2016, **1**, 1-17.
3. A. E. Gilchrist and B. A. C. Harley, *Advanced Healthcare Materials*, 2021, **n/a**, 2102130.
4. N. R. Richbourg and N. A. Peppas, *Macromolecules*, 2021, **54**, 10477-10486.
5. B. Amsden, *Macromolecules*, 1998, **31**, 8382-8395.
6. D. E. Liu, C. Kotsmar, F. Nguyen, T. Sells, N. O. Taylor, J. M. Prausnitz and C. J. Radke, *Industrial & Engineering Chemistry Research*, 2013, **52**, 18109-18120.
7. N. R. Richbourg and N. A. Peppas, *Prog Polym Sci*, 2020, **105**, 101243.
8. C. T. Reinhart and N. A. Peppas, *J Membr Sci*, 1984, **18**, 227-239.
9. N. A. Peppas and C. T. Reinhart, *Journal of Membrane Science*, 1983, **15**, 275-287.
10. J. L. Stringer and N. A. Peppas, *Journal of Controlled Release*, 1996, **42**, 195-202.
11. N. R. Richbourg, A. Ravikumar and N. A. Peppas, *Macromolecular Chemistry and Physics*, 2021, **222**, 2100138.
12. G. Ogston Alexander, B. N. Preston, J. D. Wells and J. M. Snowden, *Proceedings of the Royal Society of London. A. Mathematical and Physical Sciences*, 1973, **333**, 297-316.
13. R. J. Phillips, *Biophysical Journal*, 2000, **79**, 3350-3353.
14. L. Johansson, C. Elvingson and J. E. Loefroth, *Macromolecules*, 1991, **24**, 6024-6029.
15. Y. E. Solomentsev and J. L. Anderson, *Physics of Fluids*, 1996, **8**, 1119-1121.
16. C. Owh, V. Ow, Q. Lin, J. H. M. Wong, D. Ho, X. J. Loh and K. Xue, *Biomaterials Advances*, 2022, **141**, 213100.
17. B. D. Fairbanks, M. P. Schwartz, A. E. Halevi, C. R. Nuttelman, C. N. Bowman and K. S. Anseth, *Adv Mater*, 2009, **21**, 5005-5010.
18. A. Raza and C.-C. Lin, *Macromol Biosci*, 2013, **13**, 1048-1058.
19. M. S. Rehmann, J. I. Luna, E. Maverakis and A. M. Kloxin, *J Biomed Mater Res*, 2016, **104**, 1162-1174.
20. N. R. Richbourg, M. Wancura, A. E. Gilchrist, S. Toubbeh, B. A. C. Harley, E. Cosgriff-Hernandez and N. A. Peppas, *Science Advances*, 2021, **7**, eabe3245.
21. T. Canal and N. A. Peppas, *J Biomed Mater Res*, 1989, **23**, 1183-1193.
22. E. Axpe, D. Chan, G. S. Offeddu, Y. Chang, D. Merida, H. L. Hernandez and E. A. Appel, *Macromolecules*, 2019, **52**, 6889-6897.
23. G. S. Offeddu, E. Axpe, B. A. C. Harley and M. L. Oyen, *AIP Adv*, 2018, **8**, 1-6.
24. T. Sakai, T. Matsunaga, Y. Yamamoto, C. Ito, R. Yoshida, S. Suzuki, N. Sasaki, M. Shibayama and U.-i. Chung, *Macromolecules*, 2008, **41**, 5379-5384.
25. E. A. Phelps, N. O. Enemchukwu, V. F. Fiore, J. C. Sy, N. Murthy, T. A. Sulchek, T. H. Barker and A. J. García, *Adv Mater*, 2012, **24**, 64-70.
26. M. W. Toepke, N. A. Impellitteri, J. M. Theisen and W. L. Murphy, *Macromolecular Materials and Engineering*, 2013, **298**, 699-703.
27. S. Bernhard and M. W. Tibbitt, *Advanced Drug Delivery Reviews*, 2021, **171**, 240-256.
28. S. Lee, X. Tong and F. Yang, *Biomaterials Science*, 2016, **4**, 405-411.
29. S. Lee, X. Tong and F. Yang, *Acta Biomater*, 2014, **10**, 4167-4174.
30. M. B. Browning, T. Wilems, M. Hahn and E. Cosgriff-Hernandez, *J Biomed Mater Res, Part A*, 2011, **98A**, 268-273.
31. D. J. Munoz-Pinto, S. Samavedi, B. Grigoryan and M. S. Hahn, *Polymer*, 2015, **77**, 227-238.
32. M. S. Rehmann, K. M. Skeens, P. M. Kharkar, E. M. Ford, E. Maverakis, K. H. Lee and A. M. Kloxin, *Biomacromolecules*, 2017, **18**, 3131-3142.
33. V. Hagel, T. Haraszti and H. Boehm, *Biointerphases*, 2013, **8**, 36.
34. R. A. Hegab, S. Pardue, X. Shen, C. Kevil, N. A. Peppas and M. E. Caldorera-Moore, *Journal of Applied Polymer Science*, 2019, **137**, 48767.

35. S. Pedron, A. M. Pritchard, G. A. Vincil, B. Andrade, S. C. Zimmerman and B. A. C. Harley, *Biomacromolecules*, 2017, **18**, 1393-1400.
36. M. P. Lutolf and J. A. Hubbell, *Biomacromolecules*, 2003, **4**, 713-722.
37. C. Cha, J. H. Jeong, J. Shim and H. Kong, *Acta Biomaterialia*, 2011, **7**, 3719-3728.
38. B. G. Munoz-Robles, I. Kopyeva and C. A. DeForest, *Advanced Materials Interfaces*, 2020, **n/a**, 2001198.
39. C. Kotsmar, T. Sells, N. Taylor, D. E. Liu, J. M. Prausnitz and C. J. Radke, *Macromolecules*, 2012, **45**, 9177-9187.
40. N. A. Hadjiev and B. G. Amsden, *Journal of Controlled Release*, 2015, **199**, 10-16.
41. A. C. Jimenez-Vergara, J. Lewis, M. S. Hahn and D. J. Munoz-Pinto, *J Biomed Mater Res, Part B*, 2017, **106**, 1339-1348.
42. S. P. Zustiak, H. Boukari and J. B. Leach, *Soft Matter*, 2010, **6**, 3609-3618.